P-ISSN 2586-9000
E-ISSN 2586-9027
Homepage : https://tci-thaijo.org/index.php/SciTechAsia
Science & Technology Asia
Vol.26 No.2 April - June 2021
Page: [1-15]
Original research article

Effect of Various Shaped Al_2O_3 and TiO_2 Nanoparticles on Water-Based MHD Nanofluid Flow Through Convergent-Divergent Channels

Ashik Chandra Das, Md. Sarwar Alam*

Department of Mathematics, Jagannath University, Dhaka-1100, Bangladesh

Received 22 June 2020; Received in revised form 8 December 2020
Accepted 7 January 2021; Available online 25 June 2021

ABSTRACT

The present study inspects the effects of three different shapes of Al_2O_3 and TiO_2 nanoparticles on the two-dimensional heat transfer of steady magnetohydrodynamic incompressible water-based nanofluid flow through convergent-divergent channels. The governing dimensional partial differential equations are converted into a system of dimensionless ordinary differential equations using appropriate transformations. These dimensionless governing equations are solved applying power series and the solutions are then analysed by Hermite-Padé approximation method. The considered three shapes of nanoparticles are platelet, cylinder, and brick for performing the analysis. The influences of governing physical parameters such as channel angle, Reynolds number, Hartman number, Prandtl number, Eckert number and nanoparticles solid volume fraction on the velocity profiles and temperature distributions are investigated. The effects of three different shapes are examined for the case of all parameters and it is found that the brick-shaped nanoparticles exhibit higher temperature distributions compared to cylinder-shaped and platelet-shaped particles.

Keywords: Al_2O_3 and TiO_2-nanoparticles; Convergent-divergent channel; Hermite-Padé approximation; Magnetohydrodynamic; Shape factors

1. Introduction

The convergent-divergent channel flows have several applications in industrial, aerospace, chemical, civil, environmental, mechanical and biomechanical engineering. Moreover, there are numerous applications of this mathematical model in order to investigate the flow of rivers and canals, and the blood flow in the human body. Jeffery [1] and Hamel [2] first examined the two-dimensional flow in convergent-divergent channels, which is known as classical Jeffery-Hamel flow in fluid dynamics. Many researchers have studied this problem and a review of information related to this problem can be found in [3]. The principles of Jeffery-Hamel flow are based on the concepts that this flow is separated by a fixed angle which is driven by a source or sink at the apex. Different properties related to this problem

***Corresponding author:** sarwardu75@gmail.com **doi:** 10.14456/scitechasia.2021.21

have been investigated by several researchers which are available in [4-7]. Depending on two dimensionless parameters, the flow Reynolds number and channel angular width, these flows have the similarity solution of the Navier-Stokes Equation [8].

Magnetohydrodynamics (MHD) is concerned with the mutual interaction of fluid flow and magnetic fields. Magnetic fields influence many natural and man-made flows. They are routinely used in industry to heat, pump, stir and levitate liquid metals. The theory of MHD states that the presence of a magnetic field induced a current in a moving conductive fluid. This induced current produces the Lorentz force on ions of the conductive fluid. The investigation of MHD flow through convergent-divergent channels is not only interesting theoretically but also because of applications in mathematical modeling of several industries to design cooling system with liquid metals, MHD generators, accelerators, pumps and flow meters [9-10]. Makinde and Mhone [11] investigated the extension of the classical Jeffery-Hamel flows to MHD. They explained that in solution of the MHD flows, the effect of an external magnetic field works as a parameter in convergent-divergent channels. Makinde and Mhone [12] studied the temporal development of small disturbances in MHD Jeffery-Hamel flows using the Chebyshev spectral collection method. Moreover, Makinde [13] presented a numerical study on the effect of an arbitrary magnetic Reynolds number on steady flow of an incompressible conducting viscous liquid in a convergent-divergent channel under MHD. The solution of the nonlinear equation for the MHD Jeffery-Hamel problem was found by Mosta et al. [14] by using a novel hybrid spectral-homotopy analysis method. Another researcher Moghimi et al. [15] also solved the Jeffery-Hamel flow problem by using the homotopy perturbation method.

There is a need to develop new types of fluids that will be more effective in terms of heat exchange performance by taking into account the rising demands of modern technology, including power stations, chemical production and microelectronics. Presently, it is noticeable that the interest of the researchers is increasing in the analysis of nanofluids which have high thermal conductivity. A dilute suspension of solid nanoparticles with a base fluid was first named nanofluid by Choi [16]. Nanoparticles have unique chemical and physical properties [17] and have better thermal conductivity and radiative heat transfer compared to the base fluid only. Nanofluids are engineered dilute colloidal dispersions of nanosized (less than 100 nm) particles in a base fluid [18]. These nanoparticles behave as good conductors of heat and enable the base fluids to enhance their thermal properties. Sheikholeslami et al. [19] studied the effects of magnetic field and nanoparticles on the Jeffery-Hamel flow using a powerful analytical method which is known as the Adomian decomposition method. Moradi et al. [20] studied the effects of heat transfer and viscous dissipation on the Jeffery-Hamel flow of nanofluids. Moreover, the combined free and forced convection MHD flow in a rotating channel with perfectly conducting walls was investigated by Seth and Singh [21]. Alam et al. [22-23] and Alam and Khan [24] studied MHD Jeffery-Hamel nanofluid flow for different nanoparticles and the inherent irreversibility of the flow. Finally, Syed et al. [25] analyzed a study of velocity and temperature slip effects on the flow of water based nanofluids in converging and diverging channels.

The aim of this study is to show the effects of three different shapes; platelet, cylinder and bricks; of the Al_2O_3 and TiO_2 solid nanoparticles on velocity profiles and temperature distributions of the MHD Jeffery-Hamel flow. The influences of nanoparticles solid volume friction ϕ, channel angle α, Reynolds number Re, and Hartmann number Ha, Eckert number Ec, Prandtl number Pr on velocity profiles and temperature distributions are also examined.

2. Materials and Methods

A two-dimensional steady incompressible laminar flow of conducting water based Al_2O_3 and TiO_2 -nanofluids from a source or sink between two non-paralleled channels walls with radius r intersect at an angle 2α is considered as seen in Fig. 1. The cylindrical coordinate system (r,ϕ,z) is used and the velocity is supposed to be purely radial which depends on *r* and φ only, hence the flow controlling parameters have no variation along the *z* direction. An external magnetic field is considered to be enacted vertically downward to the top wall. Let α be the semi-angle and the domain of the flow be $-|\alpha|<\phi<|\alpha|$. The continuity equation, momentum equations and energy equation considering viscous dissipation and Joule heating in reduced polar coordinates are

$$\frac{\rho_{nf}}{r}\frac{\partial}{\partial r}(ru(r,\phi))=0, \tag{1}$$

$$u(r,\phi)\frac{\partial u(r,\phi)}{\partial r}=-\frac{1}{\rho_{nf}}\frac{\partial p}{\partial r}+\upsilon_{nf}\left(\frac{\partial^2 u(r,\phi)}{\partial r^2}+\frac{1}{r}\frac{\partial u(r,\phi)}{\partial r}+\frac{1}{r^2}\frac{\partial^2 u(r,\phi)}{\partial \phi^2}-\frac{u(r,\phi)}{r^2}\right)-\frac{\sigma_{nf}B_0^2}{\rho_{nf}r^2}u(r,\phi), \tag{2}$$

$$\frac{1}{\rho_{nf}r}\frac{\partial p}{\partial \phi}-\frac{2\upsilon_{nf}}{r^2}\frac{\partial u(r,\phi)}{\partial \phi}=0, \tag{3}$$

$$u(r,\phi)\frac{\partial \bar{T}(r,\phi)}{\partial r}=\frac{\kappa_{nf}}{(\rho c_p)_{nf}}\left(\frac{\partial^2 \bar{T}(r,\phi)}{\partial r^2}+\frac{1}{r}\frac{\partial \bar{T}(r,\phi)}{\partial r}+\frac{1}{r^2}\frac{\partial^2 \bar{T}(r,\phi)}{\partial \phi^2}\right)+\frac{\mu_{nf}}{(\rho c_p)_{nf}}\left(4\left(\frac{\partial u(r,\phi)}{\partial r}\right)^2+\frac{1}{r^2}\left(\frac{\partial u(r,\phi)}{\partial \phi}\right)^2\right)+\frac{\sigma_{nf}B_0^2}{(\rho c_p)_{nf}r^2}(u(r,\phi))^2. \tag{4}$$

It is supposed that the flow is symmetrically radial, i.e., $v=0$. The volumetric flow rate through the channel then becomes

$$Q=\int_{-\alpha}^{\alpha} urd\phi. \tag{5}$$

The corresponding boundary conditions are

$$\begin{aligned} &u(r,\varphi)=0 \quad \text{at} \quad \phi=\pm\alpha,\\ &\bar{T}=T_h \quad \text{at} \quad \phi=\alpha, \ \text{and}\\ &\bar{T}=T_c \quad \text{at} \quad \phi=-\alpha, \end{aligned} \tag{6}$$

where, B_0 is the electromagnetic induction, p is the fluid pressure and *u* is the radial velocity, ρ_{nf} is the effective density, μ_{nf} is the effective dynamic viscosity, σ_{nf} is the electrical conductivity, and υ_{nf} is the kinematic viscosity of the nanofluid.

$$\rho_{nf}=\rho_f(1-\phi)+\rho_s\phi,\ \mu_{nf}=\frac{\mu_f}{(1-\phi)^{2.5}},$$

$$\upsilon_{nf}=\frac{\mu_{nf}}{\rho_{nf}},$$

$$\frac{\sigma_{nf}}{\sigma_f}=1+\left[3\left(\frac{\sigma_s}{\sigma_f}-1\right)\varphi/\left(\left(\frac{\sigma_s}{\sigma_f}+2\right)-\left(\frac{\sigma_s}{\sigma_f}-1\right)\varphi\right)\right]. \tag{7}$$

The corresponding effective thermal conductivity and heat capacity of nanofluid are

$$\kappa_{nf}=\kappa_f\left(\frac{\kappa_s+(m+1)\kappa_f-(m+1)(\kappa_f-\kappa_s)\phi}{\kappa_s+(m+1)\kappa_f+(\kappa_f-\kappa_s)\phi}\right),\ (\rho c_p)_{nf}=(1-\phi)(\rho c_p)_f+\phi(\rho c_p)_s. \tag{8}$$

Here, ϕ is the solid volume fraction for both the nanoparticles and *m* is the shape factor. The thermophysical properties of the two nanoparticles and water are given in Table 1 and the shape factors with sphericity of nanoparticles are presented in Table 2.

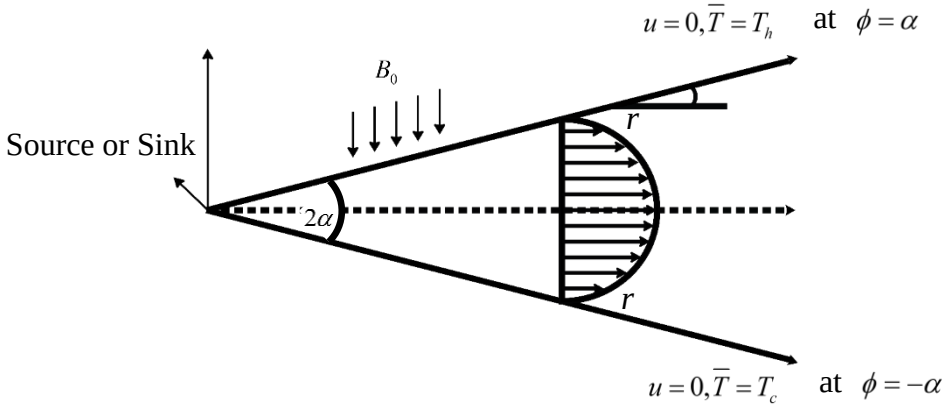

Fig. 1. Geometry of the problem.

Table 1. Thermophysical properties of water, Al_2O_3 and TiO_2 nanoparticles [23, 26].

Physical properties	Water	Al_2O_3	TiO_2
$\rho(kg/m^3)$	997.1	3970	4250
$C_p(J/kgK)$	4179	765	686.2
$\kappa(W/mK))$	0.613	40	8.9538
$\sigma(\Omega m)$	0.05	3.5 x 10^7	1.798 x 10^6

Table 2. Sphericity and shape factor of different nanoparticles [27].

Nanoparticle shapes	Aspect ratio	Sphericity	Shape factor
Platelet	1:1/18	0.52	5.7
Cylinder	1:8	0.62	4.9
Brick	1:1:1	0.81	3.7

The three different shapes of the nanoparticles are shown in Fig. 2.

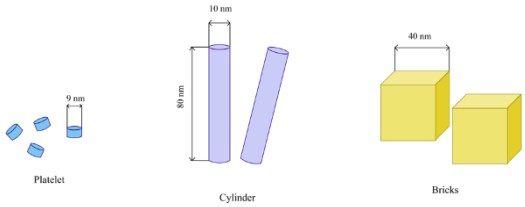

Fig. 2. Three different shapes of nanoparticles.

If it requires $Q \geq 0$, then for $\alpha > 0$ the flow is diverging from a source at $r = 0$.

Let $\psi = \psi(r, \phi)$ be the stream function, then

$$\frac{\partial \psi}{\partial \phi} = ur, \quad \frac{\partial \psi}{\partial r} = 0.$$

Now, the dimensionless variables become

$$\eta = \frac{\phi}{\alpha}, \; F(\eta) = \frac{\psi(\phi)}{Q}, \; \theta(\eta) = \frac{\overline{T} - T_c}{T_h - T_c}. \quad (9)$$

Eliminating the pressure term p from Eq. (2-3) and substituting Eq. (9) into Eq. (2-4), the velocity profiles and temperature profiles reduce to the following non-linear ordinary differential equations

$$F^{(iv)} + 2\alpha \,\mathrm{Re}\, A(1-\phi)^{2.5} F' F'' + \left(4 - (1-\phi)^{2.5}\, D\, Ha^2\right)\alpha^2 F'' = 0, \quad (10)$$

$$\theta'' + \frac{B\, Ec\, \Pr}{C(1-\phi)^{2.5}}\left[4\alpha^2 F'^2 + (F')^2 + (1-\phi)^{2.5}\, D\, Ha^2 \alpha^2 F'^2\right] = 0. \quad (11)$$

The reduced boundary conditions are

$$F = 1, \; F' = 0, \; \theta = 1 \quad \text{at} \quad \eta = 1,$$
$$F = -1, \; F' = 0, \; \theta = 0 \quad \text{at} \quad \eta = -1, \quad (12)$$

where, $\mathrm{Re} = \dfrac{Q}{\upsilon_f}$ is Reynolds number,

$\Pr = \dfrac{(\mu c_p)_f}{\kappa_f}$ is the Prandtl number,

$Ec = \dfrac{U_{\max}^2}{(c_p)_f T}$ is the Eckert number,

$Ha^2 = \dfrac{\sigma_f B_0^2}{\rho_f \upsilon_f}$ is the square of Hartmann number and α is the channel angle.

Moreover,

$$A=(1-\phi)+\frac{\rho_s}{\rho_f}\phi, \qquad B=(1-\phi)+\frac{(\rho c_p)_s}{(\rho c_p)_f}\phi,$$

$$C=\frac{\kappa_s+(m+1)\kappa_f-(m+1)(\kappa_f-\kappa_s)\phi}{\kappa_s+(m+1)\kappa_f+(\kappa_f-\kappa_s)\phi},$$

$$D=1+\left[3\left(\frac{\sigma_s}{\sigma_f}-1\right)\phi/\left(\left(\frac{\sigma_s}{\sigma_f}+2\right)-\left(\frac{\sigma_s}{\sigma_f}-1\right)\phi\right)\right]$$

are the constants.

3. Series Analysis

To solve the non-linear differential Eq. (10-11) for stream function and temperature profile, the power series expansions are considered in terms of the parameter α as follows.

$$F(\eta)=\sum_{i=0}^{\infty}F_i(\eta)\alpha^i,\ \theta(\eta)=\sum_{i=0}^{\infty}\theta_i(\eta)\alpha^i$$

as $|\alpha|<1.$ (13)

By substituting Eq. (13) into Eq. (10) and Eq. (11) along with the boundary conditions (12) and then equating the coefficient of powers of α, the first 12 coefficients of the series for stream function $F(\eta)$ and temperature $\theta(\eta)$ have been calculated using the algebraic programming language MAPLE, The first few coefficients of the series for $F(\eta)$ and $\theta(\eta)$ in terms of α, Re, *Ha*, *Ec*, Pr, ϕ, *A*, *B*, *C*, *D* are as follows:

$$\theta(\eta;\alpha,\mathrm{Re},\mathrm{Ha},\phi,\mathrm{Ec},\mathrm{Pr},\mathrm{A},\mathrm{B},\mathrm{C},\mathrm{D})=-\frac{1}{4\mathrm{C}(1-\phi)^{(5/2)}}$$
$$(1+\eta)(3\mathrm{B}\,\mathrm{Ec}\,\mathrm{Pr}\,\eta^3-3\mathrm{B}\,\mathrm{Ec}\,\mathrm{Pr}\,\eta^2+3\mathrm{B}\,\mathrm{Ec}\,\mathrm{Pr}\,\eta$$
$$-2\mathrm{C}(1-\phi)^{(5/2)}-3\mathrm{B}\,\mathrm{Ec}\,\mathrm{Pr})-\frac{3}{560\mathrm{C}}\mathrm{B}\,\mathrm{Ec}\,\mathrm{Pr}\,\mathrm{Re}\,\mathrm{A}$$
$$(9\eta^4-38\eta^2-19)(\eta-1)^2(\eta+1)^2\alpha+\mathrm{O}(\alpha^2)+...,$$
(14)

$$\mathrm{F}(\eta;\alpha,\mathrm{Re},\mathrm{Ha},\mathrm{A},\mathrm{D})=\frac{3}{2}\eta-\frac{1}{2}\eta^3-\frac{3}{280}\mathrm{Re}\,\mathrm{A}$$
$$(1-\phi)^{(5/2)}\eta(\eta^2-5)(\eta-1)^2(\eta+1)^2\alpha+(\frac{1}{431200}$$
$$\eta(\eta-1)^2(\eta+1)^2(43120+14375\,\mathrm{Re}^2\,\mathrm{A}^2\phi^4$$
$$+28750\,\mathrm{Re}^2\,\mathrm{A}^2\phi^2-2875\,\mathrm{Re}^2\,\mathrm{A}^2\phi^5)-14375\,\mathrm{Re}^2\,\mathrm{A}^2\phi$$
$$-28750\,\mathrm{Re}^2\,\mathrm{A}^2\phi^3-98\eta^6\,\mathrm{Re}^2\,\mathrm{A}^2-2472\eta^2\,\mathrm{Re}^2\,\mathrm{A}^2$$
$$+959\eta^4\,\mathrm{Re}^2\,\mathrm{A}^2-10780\sqrt{1-\phi}\mathrm{D}\,\mathrm{Ha}^2-4795\eta^4$$
$$\mathrm{Re}^2\,\mathrm{A}^2\phi+4795\eta^4\,\mathrm{Re}^2\,\mathrm{A}^2\phi^4+9590\eta^4\,\mathrm{Re}^2\,\mathrm{A}^2\phi^2-$$
$$9590\eta^4\,\mathrm{Re}^2\,\mathrm{A}^2\phi^3+98\eta^6\,\mathrm{Re}^2\,\mathrm{A}^2\phi^5+490\eta^6\,\mathrm{Re}^2$$
$$\mathrm{A}^2\varphi^5-980\eta^6\,\mathrm{Re}^2\,\mathrm{A}^2\phi^2+980\eta^6\,\mathrm{Re}^2\,\mathrm{A}^2\phi^3-$$
$$490\eta^6\,\mathrm{Re}^2\,\mathrm{A}^2\phi^4-959\eta^4\,\mathrm{Re}^2\,\mathrm{A}^2\phi^5+2472\eta^2$$
$$\mathrm{Re}^2\,\mathrm{A}^2\phi^5-24720\eta^2\,\mathrm{Re}^2\,\mathrm{A}^2\phi^2+24720\eta^2\,\mathrm{Re}^2\,\mathrm{A}^2\phi^3$$
$$-12360\eta^2\,\mathrm{Re}^2\,\mathrm{A}^2\phi^4+12360\eta^2\,\mathrm{Re}^2\,\mathrm{A}^2\varphi+$$
$$21560\sqrt{1-\phi}\mathrm{DHa}^2\phi-10780\sqrt{1-\phi}\mathrm{DHa}^2\phi^2)\alpha^2+$$
$$\mathrm{O}(\alpha^3)+.....$$
(15)

4. Numerical Computation: Hermite-Padé Approximation

In this present work, a very efficient solution method, known as Hermite-Padé approximants, which was first introduced by Padé [28] and Hermite [29] has been employed. According to this method, a function is an approximant for the series

$$S_{N-1}(\alpha)=\sum_{n=0}^{N-1}a_n\alpha^n \quad \text{as} \quad |\alpha|<1, \qquad (16)$$

if it shares with *S* the similar first few series coefficients for $|\alpha|<1$. Hence, the simplest approximants are the partial sums of the series S. When this series converges rapidly, such polynomial approximants can provide good approximations of the sum.

Consider the $(d+1)$ tuple of polynomials, where *d* is a positive integer,

$$\mathrm{P}_\mathrm{N}^{[0]},\mathrm{P}_\mathrm{N}^{[1]},...,\mathrm{P}_\mathrm{N}^{[d]},$$

where,

$$\deg P_N^{[0]}+\deg P_N^{[1]}+...+\deg P_N^{[d]}+d=N \qquad (17)$$

is a Hermite-Padé form of these series if

$$\sum_{i=0}^{d} P_N^{[i]}(\alpha) S_i(\alpha) = O(\alpha^N) \quad \text{as} \quad |\alpha| < 1 \qquad (18)$$

where $S_0(\alpha), S_1(\alpha), ..., S_d(\alpha)$ may be an independent series or different form of a single series. Now it is required to find the polynomials $P_N^{[i]}$ that satisfy the Eq. (17-18). These polynomials are totally determined by their coefficients. So, the total number of unknowns in Eq. (18) is

$$\sum_{i=0}^{d} \deg P_N^{[i]} + d + 1 = N + 1. \qquad (19)$$

Expanding the left-hand side of Eq. (18) in powers of α and equating the first N equations of the system equal to zero, a system of linear homogeneous equations can be found. To compute the coefficients of the Hermite-Padé polynomials requires some kind of normalization, such as

$$P_N^{[i]}(0) = 1 \quad \text{for some integer } 0 \le i \le d. \qquad (20)$$

It is essential to highlight that the only input required for the calculation of the Hermite-Padé polynomials are the first N coefficients of the series $S_0(\alpha), S_1(\alpha), ..., S_d(\alpha)$ Eq. (19) simply confirms that the coefficient matrix related to this system is square. In order to build the Hermite-Padé polynomials, the system of linear equations need to be solved by any standard method such as Gaussian elimination or Gauss-Jordan elimination. Drazin-Tourigney [30] Approximants are a particular kind of algebraic approximants and Khan [31] introduced a High-order differential approximant (HODA) as a special type of differential approximant. High-order partial differential approximants (HPDA) discussed in Rahman [32] are a partial differential approximant.

5. Results and Discussion

The influence of three different shapes of nanoparticles namely platelet, cylinder and bricks on velocity profiles and temperature distributions for varying values of physical parameters; nanoparticles solid volume friction ϕ, channel angle α, Reynolds number Re, Hartmann number Ha, Eckert number Ec and Prandtl number Pr is investigated in the present study. The effects of Al_2O_3- and TiO_2-nanoparticles solid volume fraction is examined at the range of $0 \le \phi \le 0.15$ for $Ha = 1$.

The dominating singularity behavior of the function $S(\alpha)$ represented by the series (16) may be written as

$$S(\alpha) \sim \begin{cases} B + A\left(1 - \dfrac{\alpha}{\alpha_c}\right)^{\delta} & \text{when } \delta \neq 0, 1, 2, ..., \\ B + A\left(1 - \dfrac{\alpha}{\alpha_c}\right)^{\delta} \ln\left|1 - \dfrac{\alpha}{\alpha_c}\right|, & \text{when } \delta = 0, 1, 2, .., \end{cases} \qquad (21)$$

As $\alpha \to \alpha_c$ where A and B are some constants and α_c is the critical point with the critical exponent δ. In order to compute the critical points, the center line axial velocity at $\eta = 0.5$ is obtained by differentiating the series (15) in the following functional form.

$$F'(\eta = 0; \alpha, \mathrm{Re}, Ha, \phi, A, D). \qquad (22)$$

The High-order differential approximant method is applied to the series (22) to compute the critical values of channel angle α_C and then to represent the comparison between present results and the published data. Table 3 shows the critical values α_C with different values of ϕ for Al_2O_3-nanoparticles. At $\phi = 0$, it is seen that the present value of α_C agrees well with the value of Alam and Khan [33] considering $d = 3$ and $N = 12$. In addition, the present value of α_C also matches with Fraenkel [34] and Makinde [13] by a minor deviation for $\phi = 0$. On the other hand, α_C decreases as ϕ increases from 0 to 0.05 and when $\phi > 0.1$, α_C increases again slightly.

Table 3. Estimated values of critical angle α_C at $\mathrm{Re}=20$ and $Ha=1$ with different values of ϕ for Al_2O_3-nanoparticles.

	Present results	Alam and Khan [33]	Fraenkel [34]	Makinde [13]
ϕ	α_C	α_C	α_C	α_C
0	0.271769	0.271769	0.269	0.269162
0.05	0.269055	-	-	-
0.1	0.271226	-	-	-
0.2	0.294968	-	-	-

5.1 Velocity profiles

The effect of channel angle α on the velocity profiles for Al_2O_3-water nanofluid in the divergent channel is demonstrated in Fig. 3. It is noticed from Fig. 3 that as the values of α increases, the velocity along the centerline increases and there occurs backflow near the channel walls. At a large value of $\alpha=30^0$, the velocity at the centerline increases rapidly and a major backflow is produced near the walls. For a diverging channel, if the channel opening enlarges, then the fully developed flow produces at the centerline and as a consequence, a major reverse flow occurs near the walls.

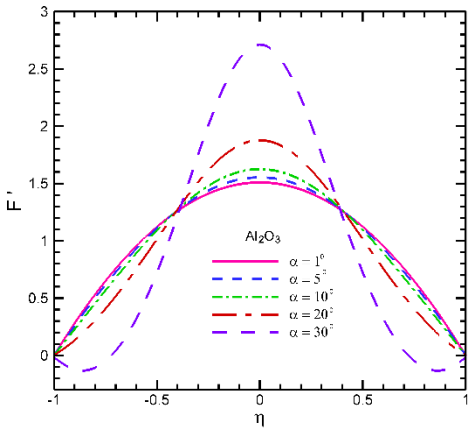

Fig. 3. Velocity profiles of Al_2O_3-water nanofluid with different values of α at $\mathrm{Re}=10, Ha=1, \phi=0.05$.

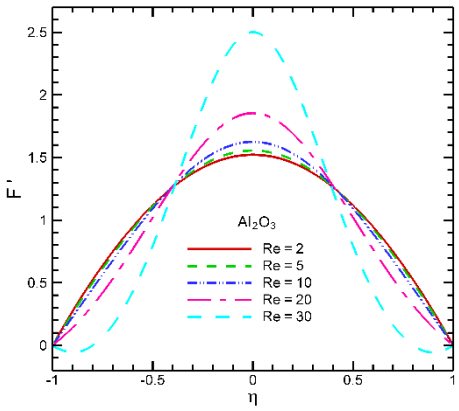

Fig. 4. Velocity profiles of Al_2O_3-water nanofluid for different values of Re at $\alpha=10^0, \mathrm{Ha}=1, \phi=0.05$.

The conjecture of Fig. 3 agreed well with the results of Alam et al. [22]. Fig. 4 illustrates the influence of Reynolds number on velocity profiles for the Al_2O_3-water nanofluid. It is consistently observed that as *Re* increases the centerline velocity increases, whereas backflow arises at the walls. The higher values of Reynolds number create more inertia forces for Al_2O_3-water nanofluid, and these forces produce fully developed flow at the centerline and a significant reverse flow at the channel walls.

According to Fraenkel [34] and Makinde [13], the critical Reynolds number for Jeffery-Hamel convergent-divergent channel flow is $\mathrm{Re}_c \approx 54.44$. It indicates that there is an onset of instability for this channel flow before $\mathrm{Re}_c \approx 54.44$. For this reason, the range of *Re* is considered between 2 and 30 for the consistency of the results.

Fig. 5 show the effect of Hartmann number *Ha* on the velocity profile for a divergent channel. It is seen that the increasing values of *Ha* reduces the velocity along the centerline $(-0.5<\eta<0.5)$ and enlarges the velocity near the left wall $(-1.0<\eta<-0.5)$ and right wall $(0.5<\eta<1.0)$ uniformly. The increasing of *Ha* tends to increase the Lorentz force due to the magnetic field and this Lorentz force

suppresses the velocity along the centerline. Figs. 6 (a-c) display the effects of Al_2O_3 and TiO_2 -nanoparticles solid volume fraction on velocity profiles. It is seen in large scale from Fig 6(a) that for Al_2O_3-nanofluid, the velocity decreases when the volume fraction ϕ increases. The nanofluids density increases when the volume fraction ϕ increases and this increasing density reduces the fluid flow significantly. Fig 6(b) displays the effect of two Al_2O_3- and TiO_2 -nanoparticles on velocity profiles at fixed $\phi = 0.05$. It is found in large scale that fluid velocity declines for Al_2O_3-nanoparticles compared to TiO_2-nanoparticles. The combined effects of Al_2O_3- and TiO_2 -nanoparticles with various values of ϕ on velocity profiles are depicted in Fig. 6(c). It is interestingly and clearly seen in large scale that at each value of ϕ, the velocity curve consistently decreases for Al_2O_3 -nanoparticles compared to TiO_2 -nanoparticles.

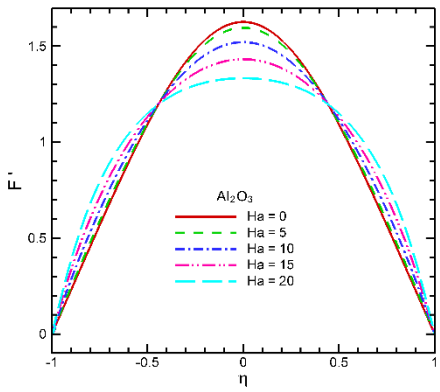

Fig. 5. Variation of velocity profiles for Al_2O_3 -water nanofluid for different values of Ha at $\alpha = 10^0, \mathrm{Re} = 10, \phi = 0.05$.

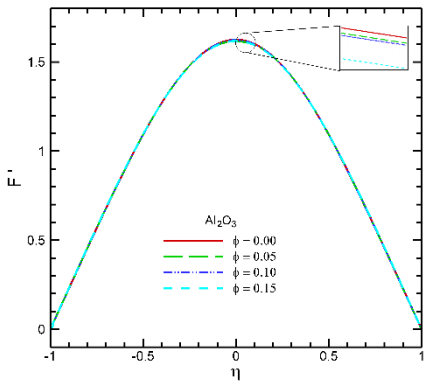

(a)

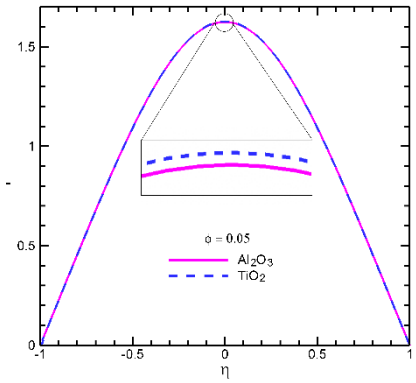

(b)

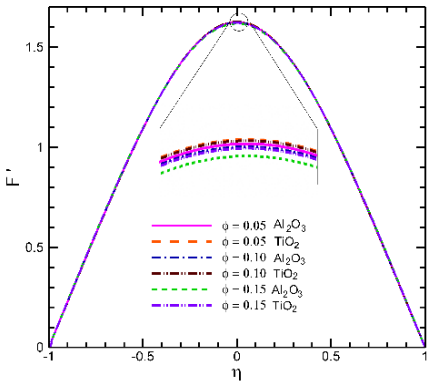

(c)

Fig. 6. Variation of velocity profiles (a) for Al_2O_3 -water nanofluid at different values of ϕ, (b) for Al_2O_3- and TiO_2 -water nanofluids with $\phi = 0.05$, and (c) for both Al_2O_3- and TiO_2 -water nanofluids with different values of ϕ at $\alpha = 10^0, \mathrm{Re} = 10, Ha = 1$.

5.2 Temperature profiles

The effect of different parameters' variation on the temperature profiles using Al_2O_3 and TiO_2 nanoparticles and considering three different shapes of these solid particles are discussed in this section.

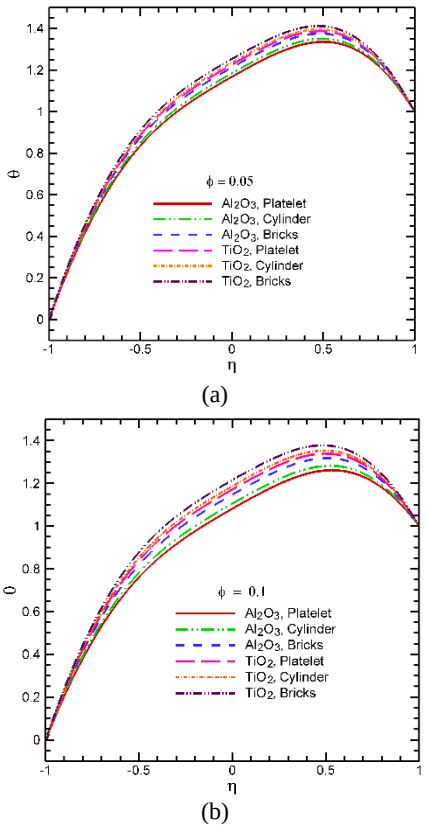

Fig. 7. Temperature profiles of Al_2O_3 and TiO_2 for (a) $\phi = 0.05$ and (b) $\phi = 0.10$ at $\alpha = 10^0$, $Ha = 1, \mathrm{Re} = 10, \mathrm{Pr} = 7.1,\ Ec = 0.1$.

Figs. 7(a-b) exhibit the variation of temperature distributions with effect of two nanoparticles Al_2O_3 and TiO_2 as well as their different shapes very significantly for $\phi = 0.05$ and $\phi = 0.10$. In Fig. 7(a) for $\phi = 0.05$, it is noticed that the temperature values of TiO_2-nanoparticles are higher than Al_2O_3-nanoparticles. The hydrophilicity of Al_2O_3-nanoparticles is stronger than the TiO_2-nanoparticles. On the other hand, the superficial roughness in the TiO_2-nanoparticles was greater than Al_2O_3-nanoparticles. The TiO_2-nanoparticles showed a greater degree of homogeneity than the Al_2O_3-nanoparticles, however Al_2O_3-nanoparticles possessed higher mechanical resistance than the TiO_2-nanoparticles. Hence the heat transfer rate of TiO_2-nanoparticles is greater than Al_2O_3-nanoparticles. Moreover, among the three shapes, brick shape nanoparticles have the highest temperature values. It is clear that the shape of platelet and cylinder have larger viscosity due to which these shapes have the lowest temperature, whereas brick shape has the highest temperature due to the least viscosity. This is due to the shear thinning behavior of the nanoparticles with temperature.

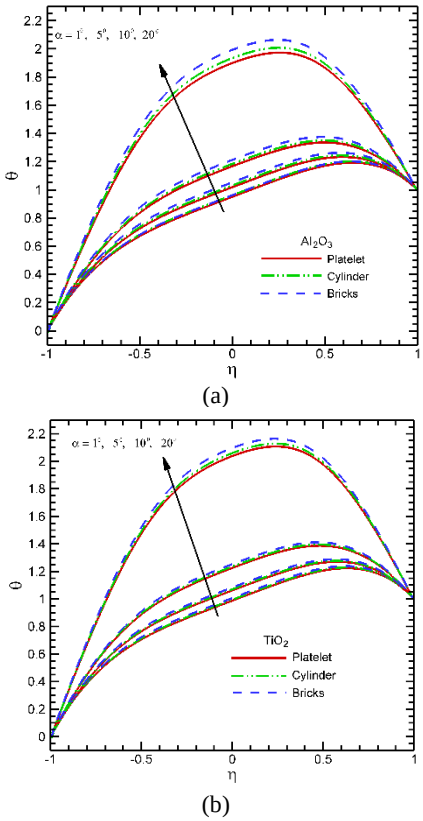

Fig. 8. Temperature profiles of (a) Al_2O_3-nanoparticles and (b) TiO_2-nanoparticles with

different values of α at $\phi = 0.05, Ha = 1,$ $\mathrm{Re} = 10, \mathrm{Pr} = 7.1, Ec = 0.1.$

On the other hand, in Fig. 7(b) for $\phi = 0.10$, similar behavior in temperature profiles is seen, but the variation in temperature distributions is more significant for the two nanoparticles and their different shape factors as the nanoparticles volume fraction ϕ increases. The influence of increasing values of α and Re on the temperature distributions is seen in Figs. 8(a-b) and Figs. 9 (a-b), respectively.

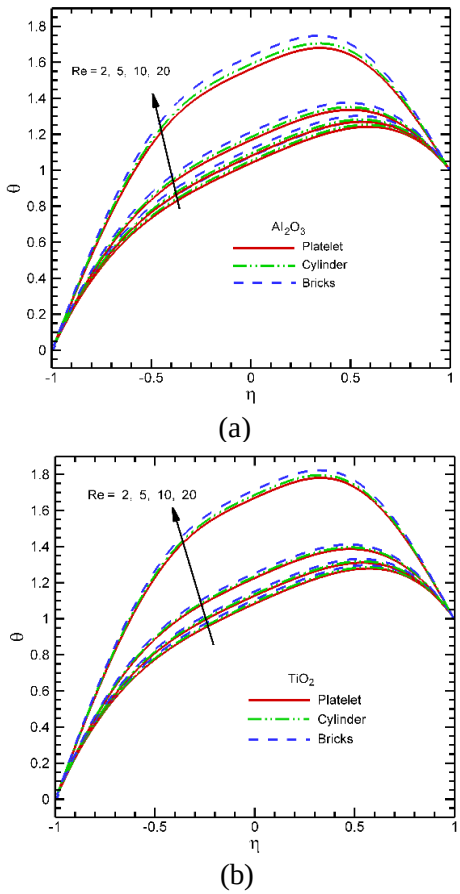

Fig. 9. Temperature profiles of (a) Al_2O_3-nanoparticles and (b) TiO_2-nanoparticles for different values of Re at $\alpha = 10^0, \phi = 0.05,$ $Ha = 1, \mathrm{Pr} = 7.1, Ec = 0.1.$

It is noticed in Fig. 8(a) and Fig. 8(b) in the way that the temperature rises massively around the channel centerline due to the increasing values of channel angle for Al_2O_3 and TiO_2 nanoparticles, respectively. The effect of flow Reynolds number Re on temperature distributions for Al_2O_3 and TiO_2-nanoparticles is depicted in Fig. 9(a) and Fig. 9(b), respectively.

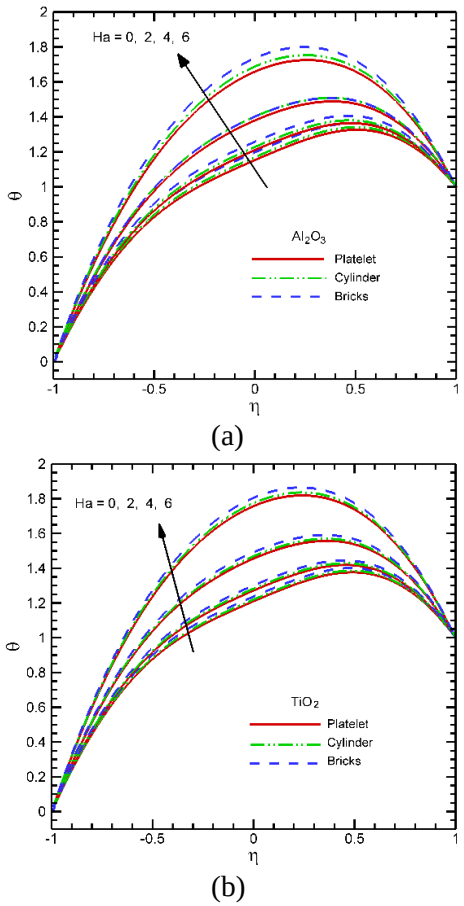

Fig. 10. Temperature profiles of (a) Al_2O_3-nanoparticles and (b) TiO_2-nanoparticles at different values of Ha at $\alpha = 10^0, \phi = 0.05, \mathrm{Re} = 10, \mathrm{Pr} = 7.1, Ec = 0.1.$

An increase in fluid temperature is noticeable around the channel centerline for rising values of *Re*. As it is already observed in Fig. 3 and Fig. 4 that the rising values of α and Re accelerates the fluid velocity around the channel centerline, hence these advanced

fluid flow produce higher temperature values consistently at this region as seen in Figs 8(a-b) and Figs 9(a-b). Furthermore, it can also be noticed that the brick shaped nanoparticles have higher temperature compared to cylinder shaped and platelet shaped nanoparticles in all cases. Figs. 10(a-b) demonstrate the impact of Hartmann number on the temperature field for the two nanoparticles. It is interesting that the temperature gets higher around the channel centerline for the increasing values of Hartmann number *Ha* due to Ohmic heating. Ohmic heating is a heating process in which heat is directly dissipated in the reaction medium, and is a high energy-efficient way of heating chemical reactions. The progress of ohmic heating depends on the electrical conductivity of the fluid and magnetic field strength.

Figs. 11(a-b) show the effects of the Eckert number on temperature field for Al_2O_3- and TiO_2-nanoparticles, respectively. It is found from Figs. 11(a-b) that for both nanoparticles, the temperature increases along the centerline for increasing values of *Ec*. The consequence due to the presence of dissipation term in energy equation is defined by the Eckert number. Meanwhile, the Eckert number is the ratio of the square of maximum velocity and specific heat.

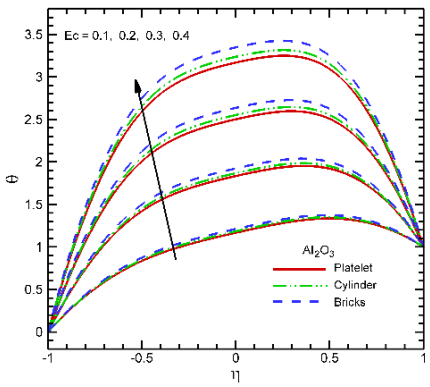

(a)

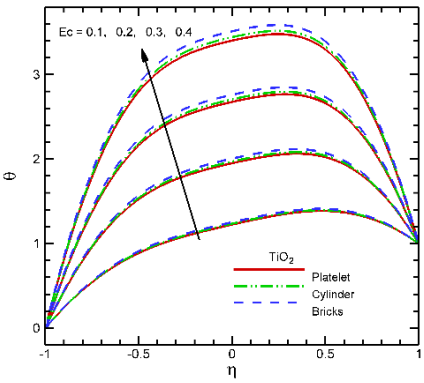

(b)

Fig. 11. Temperature profiles of (a) Al_2O_3-nanoparticles and (b) TiO_2-nanoparticles for different values of *Ec* at $\alpha = 10^0, \phi = 0.05,$ $\mathrm{Re} = 10, \mathrm{Pr} = 7.1, Ha = 1.$

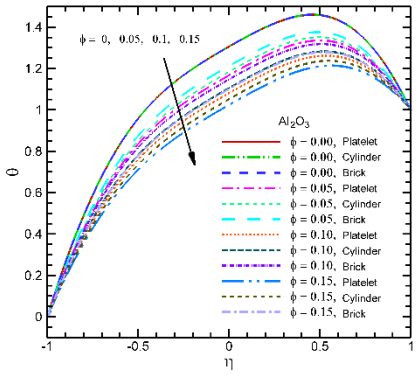

(a)

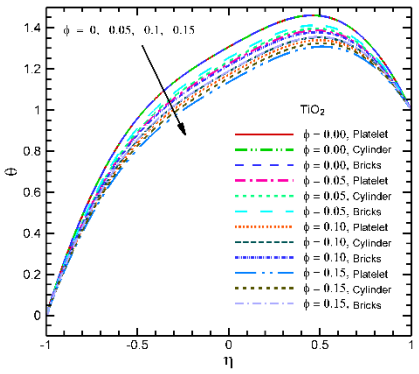

(b)

Fig. 12. Temperature profiles of (a) Al_2O_3-nanoparticles and (b) TiO_2-nanoparticles for various values of ϕ at $\alpha = 10^0, Ec = 0.1,$ $\mathrm{Re} = 10, \mathrm{Pr} = 7.1, Ha = 1.$

Accordingly, when the value of the Eckert number rises, the fluid flow rate along the centerline increases and the temperature rises at this region. The brick shaped nanoparticles display higher temperature than cylinder shaped and platelet shaped nanoparticles in all cases. The effects of nanoparticles volume fraction ϕ with various shape factors for Al_2O_3 and TiO_2 -nanoparticles are shown in Figs. 12 (a-b). It is observed that the temperature distribution reduces particularly along the channel centerline when the values of ϕ increases.

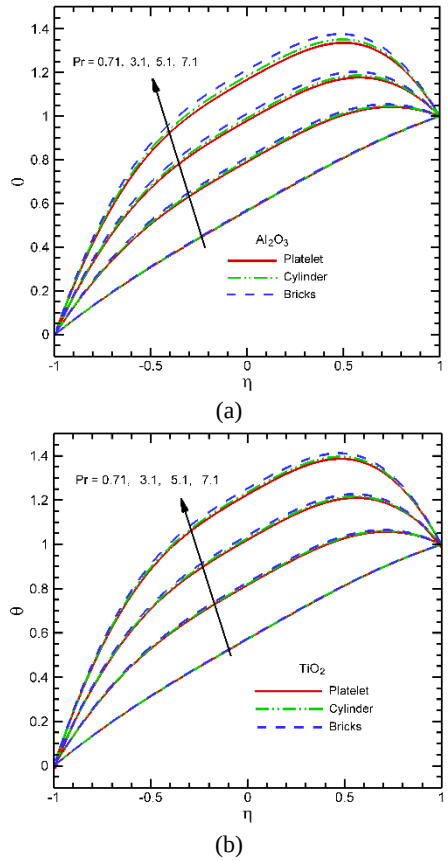

Fig. 13. Temperature profiles of (a) Al_2O_3 -nanoparticles and (b) TiO_2 -nanoparticles at various values of Pr at $\alpha = 10^0, Ec = 0.1,$ $\mathrm{Re} = 10, \phi = 0.05, Ha = 1.$

It was found in Fig. 6(a) that the velocity decreases when the volume fraction ϕ increases. Consequently, the temperature distributions also reduce due to the reduction of velocity field around this region. Variations of the Prandtl number on temperature profiles are observed in Figs. 13(a-b) for Al_2O_3 and TiO_2 -nanoparticles. It can be seen here that for the increasing value of *Pr*, the temperature becomes higher for both Al_2O_3 and TiO_2 -nanoparticles. The Prandtl number is the ratio of viscous force and thermal force. Therefore, increasing values of *Pr* increases viscosity and, hence, increases the temperature distributions of the fluid near the centerline of the channel.

6. Conclusions

The influences of three different shapes of Al_2O_3 and TiO_2 -nanoparticles on magnetohydrodynamic Jeffery-Hamel flow have been investigated in the present study. The three shapes of nanoparticles are platelet, cylinder, and brick-shaped and water is considered as the base fluid. The effects of various physical parameters on the velocity field and temperature distribution are discussed in detail. The main conclusions of this study are as follows:

- Around the centerline of the channel, the fluid velocity and temperature distribution are enhanced as the channel angle α and flow Reynolds number *Re* increase. Backflow occurs near the walls in a diverging channel as α exceeds 10^0 (i.e. at 20^0, 30^0) and *Re* surpasses 10 (i.e. at 20, 30) respectively. As the critical value $\alpha_C \approx 15.57^\circ$, this backflow behaviour arises physically. Hence, it is found that there is an onset of instability beyond these values of the parameters for this flow problem.
- The fluid velocity reduces whereas the temperature rises near the channel centerline for higher values of Hartmann number. Moreover, velocity near the two walls increases as *Ha* increases.

- Fluid velocity, as well as temperature, reduces for increasing values of the nanoparticles volume friction.
- Temperature distributions around the channel centerline get higher when the Eckert number and the Prandtl number increases.

- Nanoparticles shape factors have a significant influence on the temperature field. Brick-shaped nanoparticles exhibit higher temperature values compared to cylinder-shaped and platelet-shaped nanoparticles. Moreover, between the two nanoparticles, TiO_2-nanoparticles exhibit higher temperature values than Al_2O_3-nanoparticles. We have provided a basis for guidance regarding nanoparticles and its different shapes for MHD Jeffery-Hamel flow.

Acknowledgement

This work is done within the framework of the research project of the corresponding author under Department of Mathematics, Jagannath University, Dhaka. Financial support from the Jagannath University development project is acknowledged.

References

[1] Jeffery GB. The two-dimensional steady motion of a viscous fluid. Philosophical Magazine 1915; 6:455-65.

[2] Hamel G. Spiralförmige Bewegungen zäher Flüssigkeiten. Jahresbericht Der Deutschen Math 1916; 25:34-60.

[3] Esmaili Q, Ramiar A, Alizadeh E, Ganji DD. An approximation of the analytical solution of the Jeffery–Hamel flow by decomposition method. Physics Letters A 2008; 372:3434-9.

[4] Rosenhead L. The steady two-dimensional radial flow of viscous fluid between two inclined plane walls. Proceedings of the Royal Society A 1940; 175:436-67.

[5] Batchelor GK. An Introduction to Fluid Dynamics. Cambridge: Cambridge University Press; 1967.

[6] Sadri R. Channel entrance flow [Ph.D. thesis]. Department of Mechanical Engineering: University of Western Ontario; 1997.

[7] Hamadiche M, Scott J, Jeandel D. Temporal stability of Jeffery-Hamel flow. Journal of Fluid Mechanics 1994; 268:71-88.

[8] Makinde OD. Steady flow in a linearly diverging asymmetrical channel. Computer Assisted Mechanics and Engineering Sciences 1997; 4:157-65.

[9] Cha JE, Ahn YC, Kim MH. Flow measurement with an electromagnetic flow meter in two-phase bubbly and slug flow regimes. Flow Measurement and Instrumentation 2002; 12:329-39.

[10] Tendler M. Confinement and related transport in extrap geometry. Nuclear Instruments and Methods in Physics Research 1983; 207:233-40.

[11] Makinde OD, Mhone PY. Hermite-Pade' Approximation approach to Hydromagnetic flows in convergent-divergent channels. Applied Mathematics and Computation 2006; 181:966-72.

[12] Makinde OD, Mhone PY. Temporal stability of small disturbances in MHD Jeffery-Hamel flows, Computers and Mathematics with Applications 2007; 53:128-36.

[13] Makinde OD. Effect of arbitrary magnetic Reynolds number on MHD flows in convergent divergent channels. International Journal of Numerical Method for Heat & Fluid Flow 2008; 18:697-707.

[14] Motsa SS, Sibanda P, Awad FG, Shateyi S. A new spectral-homotopy analysis method for the MHD Jeffery-Hamel

problem. Computers & Fluids 2010; 39:1219-25.

[15] Moghimia SM, Ganji DD, Bararnia H, Hosseini M, Jalaal M. Homotopy perturbation method for nonlinear MHD Jeffery–Hamel Problem. Computers and Mathematics with Applications 2011; 61:2213-16.

[16] Choi SUS. Enhancing thermal conductivity of fluids with nanoparticles. In Proceedings of the 1995 ASME International Mechanical Engineering Congress and Exposition 1995; 66:99-105.

[17] Das SK, Choi SUS, Patel HE. Heat transfer in nanofluids-A review. Heat Transfer Engineering 2006; 27:3-19.

[18] Das SK, Choi SUS, Yu W, Pradeep T. New York: Nanofluids: Science and Technology; 2007.

[19] Sheikholeslami M, Ganji DD, Ashorynejad HR, Rokni HB. Analytical investigation of Jeffery-Hamel flow with high magnetic field and nanoparticle by Adomian decomposition method. Applied Mathematics and Mechanics English Edition 2012; 33:25-36.

[20] Moradi A, Alsaedi A, Hayat T. Investigation of heat transfer and viscous dissipation effects on the Jeffery-Hamel flow of nanofluids. Thermal Science 2015; 19:563-78.

[21] Seth GS, Singh MK. Combined free and forced convection MHD flow in a rotating channel with perfectly conducting wall. Indian Journal of Theoretical Physics 2008; 56:203-22.

[22] Alam MdS, Khan MAH, Alim MA. Magnetohydrodynamic Stability of Jeffery-Hamel Flow using Different Nanoparticles. Journal of Applied Fluid Mechanics 2016; 9:899-908.

[23] Alam MdS, Khan MAH, Makinde OD. Magneto-Nanofluid Dynamics in Convergent-Divergent Channel and Its Inherent Irreversibility. Defect and Diffusion Forum 2017; 377:95-110

[24] Alam MdS, Khan MAH. Analysis of Magnetohydrodynamic Jeffery-Hamel flow with nanoparticle by Hermite- Padé approximation technique. International Journal of Engineering, Transaction A: Basics 2015; 28:599-607.

[25] Syed TM, Khan U, Ahmed N, Sikander W. A study of Velocity and Temperature slip effects on flow of water based nanofluids in Converging and Diverging Channels. International Journal of Applied and Computational Mathematics 2015; 569-87.

[26] Alam MdS, Makinde OD, Khan MAH. Instability of variable thermal conductivity magnetohydrodynamic nanofluid flow in a vertical porous channel of varying width. Defect and Diffusion Forum 2017; 378:85-101.

[27] Mohyud-Din ST, Khan U, Hassan S. Numerical investigation of magneto-hydrodynamic flow and heat transfer of copper-water nanofluid in a channel with non-parallel walls considering different shapes of nanoparticles. Advanced in Mechanical Engineering 2016; 8:1-9.

[28] Padé H. Sur la représentation approchée d'une fonction pourdes fractions rationnelles. Annales scientifiques de l'École Normale Supérieure 1892; 9:1-93.

[29] Hermite C. Sur la généralisation des fractions continues algébriques. Annali di Mathematica Pura e Applicata 1893; 21:289-308.

[30] Drazin PG, Tourigny Y. Numerical study of bifurcation by analytic continuation of a function defined by a power series. SIAM Journal of Applied Mathematics 1996; 56:1-18.

[31] Khan MAH. High-Order Differential Approximants. Journal of Computational

and Applied Mathematics 2002; 149:457-68.

[32] Rahman MM. A New Approach to Partial Differential Approximants [M. Phil thesis]. Dhaka: Bangladesh University of Engineering & Technology; 2004.

[33] Fraenkel LE, Laminar flow in symmetrical channels with slightly curved walls. I: On the Jeffery-Hamel solutions for flow between plane walls. Proc. R. Soc. London 1962; 267: 119-38.

[34] Alam MdS, Khan MAH, Critical behaviour of the MHD flow in convergent-divergent channels. Journal of Naval Architecture and Marine Engineering 2010;7(2): 83-93.